Color and Vector Flow Imaging in Parallel Ultrasound With Sub-Nyquist Sampling

Craig Madiena, Julia Faurie, Jonathan Porée, and Damien Garcia

***Abstract*— RF acquisition with a high-performance multichannel ultrasound system generates massive data sets in short periods of time, especially in "ultrafast" ultrasound when digital receive beamforming is required. Sampling at a rate four times the carrier frequency is the standard procedure since this rule complies with the Nyquist-Shannon sampling theorem and simplifies quadrature sampling. Bandpass sampling (or undersampling) outputs a bandpass signal at a rate lower than the maximal frequency without harmful aliasing. Advantages over Nyquist sampling are reduced storage volumes and data workflow, and simplified digital signal processing tasks. We used RF undersampling in color flow imaging (CFI) and vector flow imaging (VFI) to decrease data volume significantly (factor of 3 to 13 in our configurations). CFI and VFI with Nyquist and sub-Nyquist samplings were compared *in vitro* and *in vivo*. The estimate errors due to undersampling were small or marginal, which illustrates that Doppler and vector Doppler images can be correctly computed with a drastically reduced amount of RF samples. Undersampling can be a method of choice in CFI and VFI to avoid information overload and reduce data transfer and storage.**

***Index Terms*— Color Doppler, parallel ultrasound imaging, sub-Nyquist sampling, undersampling, vector Doppler, vector flow imaging (VFI).**

I. Introduction

COLOR flow imaging (CFI) and vector flow imaging (VFI) by Doppler ultrasound is experiencing a renewed interest due to the growing use of parallel ultrasound imaging at very high frame rates (ultrafast ultrasound) [1], [2]. To mention just a few *in vivo* 2-D applications, ultrafast CFI and VFI were implemented for functional brain imaging [3], intraoperative cardiac and epiaortic flow imaging [4], and Doppler vortography [5]. Feasibility of 3-D ultrafast CFI and VFI has also been recently demonstrated [6]–[8]. These modalities are all based on the transmits of large ultrasound wavefronts whose backscattered signals are received with a large aperture and digitally beamformed to generate the images. In digital beamforming, the raw signals from several channels and from multiple transmits are provisionally stored before being delayed and coherently summed by parallel processing. The backscattered ultrasound RF signals are sampled by the analog-to-digital converter (ADC) typically at a sampling rate four times the carrier frequency. An RF signal centered at 5 MHz is thus usually sampled at 20 MHz. Even with a 200% bandwidth, this "four-time rule" complies with the Shannon–Nyquist theorem [9]. Four times sampling, however, can lead to substantial amounts of data in parallel ultrasound imaging. For example, in vascular echography with a 5 MHz 128-element phased-array and a 14-b resolution ADC, receiving with a full aperture and digitizing at four times the carrier frequency (i.e., $f_c = 20$ MHz) yields to an output data flow of $128 \times 20 \times 10^6 \times 14/8 \approx 4.4$ GB/s. By way of comparison, the transfer rate of the PCIe in the Verasonics Vantage is 6.6 GB/s [10]. Of particular concern, the power consumption of the ADC, and thus its sampling rate, needs to be kept as low as possible for handheld wireless ultrasound scanner operating on a battery [11]. The use of large linear (192 to 256 elements) or matrix (32×32) arrays can be memory- and power-intensive in the context of parallel ultrasound imaging. The objective of our study was to show that RF undersampling can be used to reduce data amount in CFI and VFI without significantly affecting accuracy of velocity measures.

Since coherent compounding is the key process in parallel ultrasound [1], large data sets are stored in the digital core for further processing. In light of the above, four times sampling can limit specific applications requiring: 1) high center frequencies (>20 MHz) [10], [12]; 2) massive volumes of data (e.g., 3-D ultrasound) [13]; or 3) limited transfer rate and/or limited power performance (e.g., handheld and portable scanners, wireless transducers) [11]. When dealing with bandpass signals, sub-Nyquist sampling rates can be used to alleviate data storage, signal processing, power consumption, and cost [14]. Ultrasound signals are precisely band limited, with most of the contents lying in a frequency range (f_L, f_U). This is especially true in color Doppler where long pulses (typically 8 to 16 wavelengths [15]) are transmitted to decrease the Doppler variance [16]. Such bandpass signals can be uniformly sampled at a rate lower than twice the upper frequency f_U, without loss of information, as long as the

Manuscript received January 31, 2018; accepted March 19, 2018. Date of publication March 21, 2018; date of current version May 7, 2018. This work was supported in part by the Natural Sciences and Engineering Research Council of Canada under Grant RGPAS-477914-2015 and Grant RGPIN-04217-2015, in part by the Fonds de Recherche du Québec–Nature et Technologies under Grant 2016-PR-189822, and in part by the LABEX CeLyA, Lyon, France. *(Corresponding author: Damien Garcia.)*

C. Madiena and J. Porée were with the CRCHUM, Research Center, University of Montreal Hospital, Montreal, QC H2X 0A9, Canada.

J. Faurie is with the CRCHUM, Research Center, University of Montreal Hospital, Montreal, QC H2X 0A9, Canada.

D. Garcia was with the Department of Radiology, Radio-Oncology, and Nuclear Medicine, University of Montreal, Montreal, QC H3T 1J4, Canada. He is now with CREATIS, U1206, UMR 5220, University of Lyon, F-69621, Lyon, France (e-mail: garcia.damien@gmail.com; damien.garcia@inserm.fr).

This paper has supplementary downloadable material at http://ieeexplore.ieee.org, provided by the authors.

Digital Object Identifier 10.1109/TUFFC.2018.2817885

positive and negative frequency components do not overlap. A common procedure is to sample the signals in a quadrature mode (quadrature sampling) [17]. In quadrature sampling, the signal is directed toward two samplers (I and Q channels), generally both working at a rate of f_c. A more general sub-Nyquist approach consists in sampling the bandpass signal at a rate which does not produce harmful aliasing, i.e., without frequency overlap (bandpass sampling, [14]). Tortoli *et al.* [18] have described the benefits of RF bandpass sampling in continuous-wave ultrasound Doppler twenty years ago. In the *in vitro* and *in vivo* studies described in this paper, we analyzed the impact of RF bandpass sampling on the accuracy of color Doppler and vector Doppler with ultrasound plane/diverging wave imaging. To significantly reduce data storage and avoid data overload in digital postprocessing, undersampling ratios as low as 1:13 were specifically tested. We observed that the errors in high-frame-rate color Doppler and vector Doppler induced by RF undersampling were small to marginal.

II. Methods

Bandpass sampling was investigated *in vitro* on B-mode and color Doppler imaging. It was also tested *in vitro* and *in vivo* on VFI. Doppler ultrasound images were obtained using transmits of plane or circular waves, respectively, with a linear or phased array.

A. Bandpass Sub-Nyquist Sampling

For a bandpass signal of bandwidth $B = f_U - f_L$, a frequency sampling f_s that obeys the inequality

$$\frac{2f_U}{k} \leq f_s \leq \frac{2f_L}{k-1} \tag{1}$$

with k an integer subject to $1 \leq k \leq f_U/B$, avoids harmful aliasing [14], [19]. For example, the sampling frequency for an RF signal centered at 2.5 MHz, with of bandwidth of 1 MHz, can be in $\{2\} \cup [3, 4] \cup [6, +\infty[$ MHz. A "4/5 sampling" (carrier frequency $\times$ 4/5 = 2 MHz) could thus be used under this condition. From (1), it can be shown that the lowest acceptable bandpass sampling frequency is

$$f_s = \frac{2f_U}{\lfloor f_U/B \rfloor} \tag{2}$$

where $\lfloor\ \rfloor$ denotes the floor function. In particular, a sampling frequency that satisfies inequality (1) is the following (see [18] and [20, eqs. (2)–(13)]):

$$f_s = \frac{4f_c}{k_{\text{odd}}} \tag{3}$$

where k_{odd} is an odd integer, and $f_c = (f_U + f_L)/2$ is the center frequency. To ensure that $f_s \geq 2B$, k_{odd} must satisfy

$$k_{\text{odd}} \leq \left\lfloor \frac{2f_c}{B} \right\rfloor. \tag{4}$$

The *in vitro* and *in vivo* RF ultrasound data were sampled by a Verasonics scanner (V-1-128, Verasonics Inc.) using the default 4$\times$ sampling rule (i.e., sampling frequency = center frequency $\times$ 4). The raw RF signals were bandpass-filtered (10th order Butterworth filter) between $f_c \pm B_t/2$, B_t ($> B$) being the bandwidth of the transducer at -10 dB (as given by the manufacturer). To simulate undersampling, the RF signals were then downsampled by keeping every k_{odd}th sample, starting with the first sample. The maximum k_{odd} was chosen in accordance with inequality (4). Fig. 1 illustrates two examples of RF downsampling for $k_{\text{odd}} = 3$ and $k_{\text{odd}} = 7$. The downsampled RF signals were digitally demodulated to get the I/Q components before receive beamforming and B-mode or Doppler processing (Fig. 2). A 10th-order Butterworth low-pass filter, with a normalized cutoff frequency of $B/f_s = k_{\text{odd}}B/(4f_c)$, was used in the demodulation process.

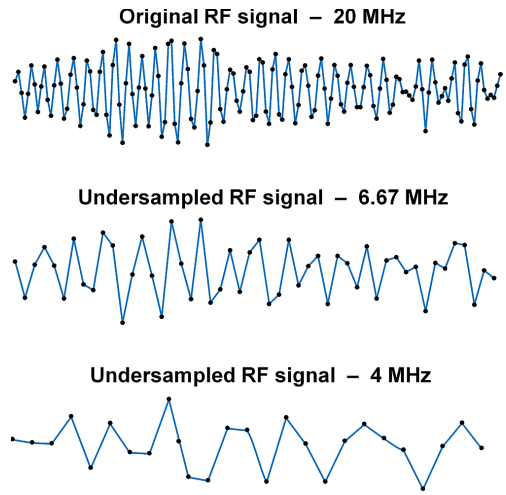

Fig. 1. RF undersampling using 4/3 sampling (second row) and 4/5 sampling (third row). The sampling rates were chosen according to (3) and (4).

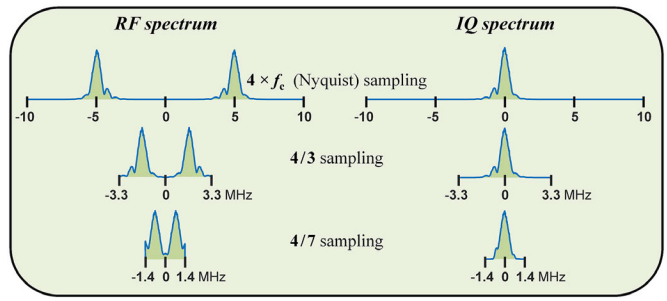

Fig. 2. RF undersampling using 4/3 sampling (second row) and 4/7 sampling (third row). Using a 4/k_{odd} sampling, with k_{odd} an odd integer subject to inequality (4), avoids significant overlapping of the positive and negative frequency components.

B. 4/3 Sampling in B-Mode Imaging—In Vitro

The 4/3 sampling ($k_{\text{odd}} = 3$) is proposed on the Verasonics Vantage. This configuration allows undersampling of RF signals with relative bandwidth less than 67% [10]. The effect of 4/3 sampling was first analyzed on B-mode images generated by plane wave imaging with a 5-MHz linear-array transducer (ATL L7-4, bandwidth at -3 and -10 dB = 42% and 88%). For this subsidiary test, we reprocessed the *in vitro* data published in [21], before (f_s = 20 MHz, 4$\times$ sampling) and after undersampling (f_s = 6.67 MHz, 4/3 sampling). In [21], the RF data were acquired in a nonmoving Gammex phantom (403GS LE, Gammex Inc.). The phantom was

insonated by successive tilted planar wavefronts with an angular increment of 1°. Contrast and lateral resolution were, respectively, determined on a 3-cm-deep anechoic target and a 1-cm-deep 0.1-mm nylon fiber. The compounding angular ranges were $[-\theta_{\max}; +\theta_{\max}]$ with a step of 1°, and $\theta_{\max}$ was varied from 0° to 10° (i.e., maximal number of compounding angles = 21). The evaluation metrics for contrast and lateral resolution were the contrast-to-noise ratio (CNR) and full width at half maximum (FWHM). More details are given in [21].

C. Undersampling in Color Doppler—In Vitro

CFI with undersampled RF signals was investigated on a 3-cm-diameter tissue-mimicking disc. This setup had the advantage to provide a ground-truth velocity field. The disc was mounted on a step motor regulating its rotational speed [22]. The phantom rotated at angular velocities of 2 to 15 revolutions per second (with an increment of 0.5), which gave a maximum outer speed of ~1.4 m/s. The disc was insonated with unsteered plane waves transmitted by a 5-MHz linear-array transducer (ATL L7-4). We used long ultrasound pulses (7 wavelengths) to reduce Doppler variance so that the signal bandwidth at −10 dB was 0.75 MHz (15%). The rotating disc was imaged using a staggered double-pulse repetition frequency (PRF) pulsing sequence to extend the Nyquist Doppler velocity, with $\mathrm{PRF}_1 = 10\,000$ Hz and $\mathrm{PRF}_2 = 2/3\ \mathrm{PRF}_1 = 6667$ Hz (see [22] for details). The corresponding extended Nyquist velocity was 1.54 m/s. The original RF signals were sampled at 20 MHz (4× sampling), then downsampled with $k_{\mathrm{odd}} = 1, 3, 5, \ldots 13$ [see (3)] to simulate ADC undersampling. After I/Q demodulation and beamforming, the Doppler velocities were estimated from the I/Q components using a 2-D autocorrelator [23] and a packet size of 17 (i.e., 8 pulse pairs for each individual PRF, see [22]). No clutter filtering was required. The color Doppler fields were compared with the ground-truth axial velocities for each rotation speed and k_{odd} integer (total of $29 \times 7 = 203$ Doppler fields). The spatially averaged absolute and relative errors were calculated. The latter were reported with respect to the outer speed (= disk angular velocity × disk radius).

A second series of *in vitro* color Doppler data were analyzed. Those experimental data were obtained in a free water jet flow generated by a sharp-edged circular orifice plate (details in [22]). The flow rate was controlled by a centrifugal pump (Micropump 75211-62, Cole-Parmer, Canada) and was varied from 3.5 to 5.5 L/min with a step of 0.2 L/min (11 experiments). The maximum jet speed was ~1.15 m/s. A 2.5-MHz phased-array transducer (ATL P4-2) was used to transmit diverging circular wavefronts. The phased-array transducer was positioned parallel to the jet and the flow was directed toward the transducer. The angular width of the insonated sector was 30°. The signal bandwidth was 1 MHz (40%), given a maximal k_{odd} integer of 5 (4). The flow jet was imaged using a dual-PRF scheme with $\mathrm{PRF}_1 = 5000$ Hz and $\mathrm{PRF}_2 = 2/3\ \mathrm{PRF}_1 = 3333$ Hz (see [22] for details) resulting in an extended Nyquist velocity of 1.6 m/s. The original RF signals were sampled at 10 MHz (4× sampling), then downsampled using $k_{\mathrm{odd}} = 5$ [i.e., $f_s = 2$ MHz, see (3)]. The Doppler velocities were obtained as described above. The color Doppler fields obtained with the 4/5 sampling were compared with those retrieved from the 4× sampling (no ground-truth was available).

D. Undersampling in Vector Flow Imaging—In Vitro and In Vivo

Undersampling was finally applied in VFI [2], both *in vitro* and *in vivo*. The rotating disk mentioned earlier was used to produce *in vitro* VFI. The ultrasound transmit sequences (unsteered plane waves with a dual-PRF scheme) and the downsampling + demodulating process were similar as those described in the preceding paragraph. Only the 4× sampling and the optimal undersampling ($k_{\mathrm{odd}} = 13$, $f_s = 1.5$ MHz) were analyzed. Two receive subapertures were used to generate the vector flow images [24]–[26], with a receive f-number of 3. The receive beam angles were ±15°. The Doppler velocities were estimated from the beamformed I/Q components using a 2-D autocorrelator and a packet size of 17 (i.e., 8 pulse pairs for each individual PRF), as mentioned earlier. The Doppler-derived velocity vectors (total of $29 \times 2 = 58$ vector Doppler fields) were compared with the ground-truth vector fields. The vector fields were not postprocessed (no smoothing).

In vivo vector flow images of the carotid bifurcation were also produced in a volunteer. We used the 5-MHz linear-array transducer (ATL L7-4) and a duplex sequence (B-mode and Doppler, successively). Eleven steered plane waves (transmit beam angles evenly spaced between −15° and 15°) were transmitted at a PRF of 5 kHz to create one coherently compounded B-mode image. Regarding vector Doppler flow imaging, 39 unsteered plane waves were transmitted through a dual-PRF scheme ($\mathrm{PRF}_1 = 5000$ Hz and $\mathrm{PRF}_2 = 3333$ Hz; 20 pulse pairs for each individual PRF). With this sequence, 82 duplex (B-mode + vector flow) images per second were obtained. The receive beamforming method to generate the vector flow images was similar as that described above (*in vitro*). A spatially adaptive polynomial regression filter, based on the corrected Akaike's information criterion [27], was used to remove the clutter components, as described in our previous study [22]. The respective signal bandwidths for B-mode and VFI were 3.3 MHz (66%, 2-cycle Tx pulses) and 0.9 MHz (18%, 8-cycle Tx pulses). The B-mode RF signals were thus downsampled at 6.7 MHz ($k_{\mathrm{odd}} = 3$), and the Doppler RF signals at 1.8 MHz ($k_{\mathrm{odd}} = 11$), to simulate undersampling. Since no ground-truth was available, the velocity vector fields of the carotid bifurcation produced from the undersampled RF signals were compared with those obtained using the standard 4× sampling (one cardiac cycle, total of 110 frames). No vector smoother was applied for quantification of the differences.

III. Results

A. Contrast and Lateral Resolution With 4/3 Sampling

As anticipated [21], contrast and lateral resolution both improved as the number of compounding angles

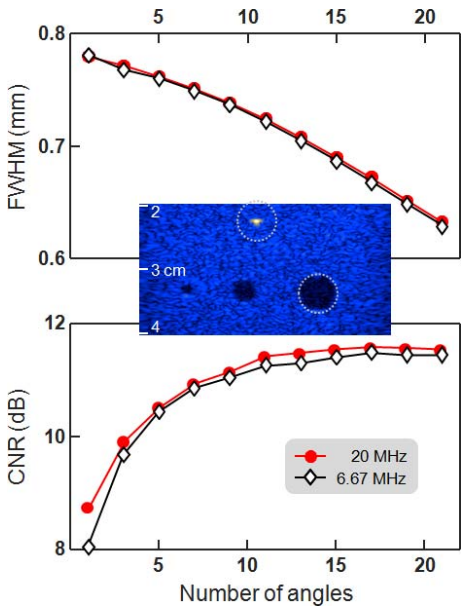

Fig. 3. Contrast (bottom panel) and lateral resolution (top panel) in coherent compound plane wave imaging. As expected, an improvement was observed as the number of compounding angles increased. No significant difference was noticed between the 4/3 sub-Nyquist sampling (diamonds) and the standard 4× sampling (dots).

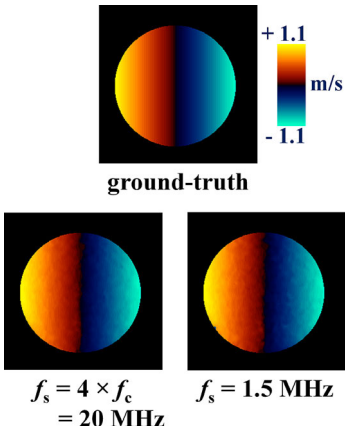

Fig. 4. *In vitro* comparison between the standard 4× sampling and the 4/13 sampling on color Doppler. The center frequency was 5 MHz. This example was obtained with the disc rotating at 11.5 rotations/s.

increased (Fig. 3). Bandpass sampling did not affect CNR nor FWHM: no difference was noticed between the 4× and 4/3 sampling approaches (Fig. 3). Although we tested the 4/3 sampling for B-mode imaging with a 5-MHz ultrasound transducer, it must be noted that this technique would be more appropriate for high-frequency transducers since the relative bandwidth is generally smaller [10].

B. Effect of Undersampling on Color Doppler

RF undersampling had very little adverse effect on color Doppler with plane wave imaging. Fig. 4 illustrates two Doppler fields measured in the rotating disk; one obtained with the original 4× sampling ($f_s = 20$ MHz), the other with a 4/13 sampling ($f_s = 1.5$ MHz). As illustrated on Fig. 5, RF undersampling induced a slight increase in the absolute

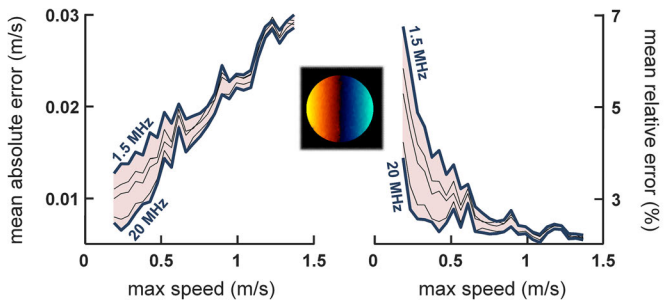

Fig. 5. Effect of RF undersampling on color Doppler in an *in vitro* rotating disc. The RF sampling was varied from 20 (4× sampling) down to 1.5 MHz (4/13 sampling). The inset represents a color Doppler image obtained with the 4/13 sampling (see Fig. 4). The center frequency was 5 MHz.

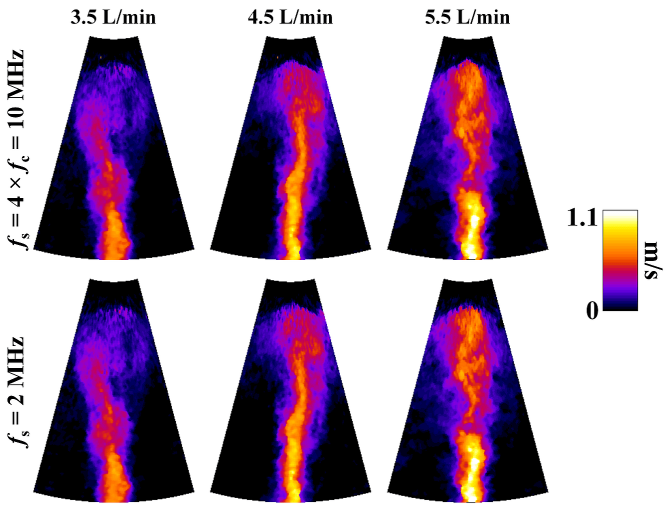

Fig. 6. Doppler velocities by high-frame-rate color Doppler, with diverging waves, in a free jet flow. First row: with the standard 4× RF sampling. Second row: with a 4/5 sampling. The center frequency was 2.5 MHz. See also the movie in the online supplemental content.

and relative errors. The respective absolute and relative errors increased from 0.007 up to 0.013 m/s and from 4% up to 7% for the smallest rotation speed (140 r/min, outer speed = 0.2 m/s). These errors were in part due to the out-of-bandwidth signals, which overlapped with the in-bandwidth signal during undersampling. Degradation of color Doppler due to RF undersampling became marginal as the velocities increased (see Fig. 5). The effect of RF undersampling (4/5 sampling: 2 versus 10 MHz) on high-frame-rate color Doppler in the free flow jet was negligible. On average, the relative difference (with respect to the maximal jet velocity) between the Doppler velocities issued, respectively, from the 4× and 4/5 samplings was $0.49 \pm 0.15\%$ (Fig. 6).

C. Effect of Undersampling on Vector Flow Imaging—In Vitro

As with color Doppler, the vector flow fields in the rotating disc based on 4× or sub-Nyquist RF sampling were very concordant (Figs. 7 and 8). The errors for the z-(axial) components were expectedly similar (<7%) as those observed with color Doppler (see Figs. 5 and 8). The errors on the

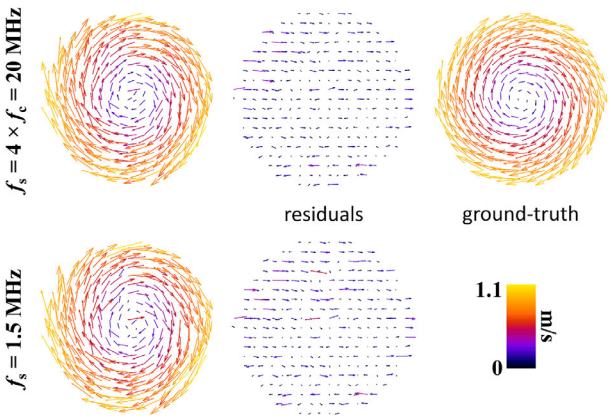

Fig. 7. VFI by high-frame-rate plane wave imaging in a spinning disc. First row: with the standard 4× RF sampling. Second row: with a 4/13 sampling. The center frequency was 5 MHz. This example was obtained with the disc rotating at 11.5 rotations/s (see also Fig. 4).

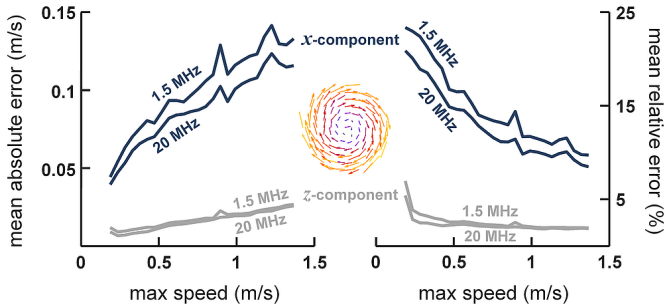

Fig. 8. Effect of RF undersampling on VFI by high-frame-rate plane wave imaging in a spinning disc. The RF sampling was varied from 20 (4× sampling) down to 1.5 MHz (4/13 sampling). The inset represents a vector Doppler image obtained with the 4/13 sampling (see Fig. 7). The center frequency was 5 MHz.

x-(cross-range) components were 4 to 5 times greater than those in the x-direction due to the lower lateral resolution. As illustrated on Fig. 8, RF undersampling induced a slight increase in the absolute and relative errors. The largest relative errors for the x-components were 21% (4× sampling) and 23% (4/13 sampling), which occurred at low rotation speeds. As speed increased, the relative x-errors tended toward 10%. Overall, RF undersampling had little impact on VFI.

D. Effect of Undersampling on Vector Flow Imaging—In Vivo

The vector flow images obtained in the carotid bifurcation showed that RF undersampling was also well adapted to *in vivo* VFI. Fig. 9 shows a snapshot (4× versus 4/11 sampling) where a vortex is visible in the carotid sinus. In Fig. 9, the vector fields were smoothed automatically [28], [29] to improve flow rendering. The overall 2-D distribution of the relative differences (with respect to the maximal speed) between the 4× and 4/11 samplings is illustrated on Fig. 10. This distribution includes the pointwise errors measured on the 110 frames during a cardiac cycle. The relative difference of the z-components was in the ± 2% range for 75% of the data (Fig. 10). With regard to the x-components, 75% of the vectors lied in the ± 10% error range.

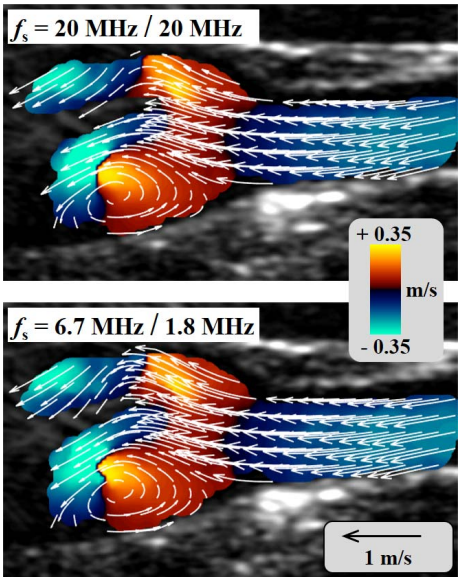

Fig. 9. VFI by high-frame-rate plane wave imaging in a carotid bifurcation. Standard 4× RF sampling ($f_s = 20$ MHz) (top). 4/3 sampling for B-mode imaging ($f_s = 6.7$ MHz) and 4/11 sampling for vector Doppler ($f_s = 1.8$ MHz) (bottom). The center frequency was 5 MHz. The color Doppler image on the background was obtained with transmit/receive beam angles of 0°/15°. See also the movie in the online supplemental content.

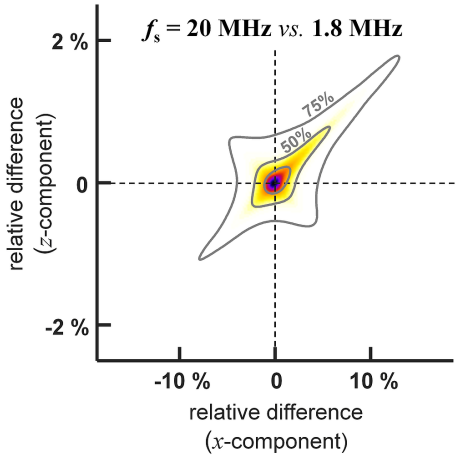

Fig. 10. VFI by high-frame-rate plane wave imaging in a carotid bifurcation. 2-D distribution of the relative differences between the vector components obtained with a 4× sampling ($f_s = 20$ MHz) and those with a 4/11 sampling ($f_s = 1.8$ MHz). See also Fig. 9. x-direction refers to lateral direction. z-direction refers to axial direction.

IV. Discussion

The *in vitro* and *in vivo* results showed that RF bandpass sampling was well adapted to color Doppler and vector Doppler imaging. Marginal or small differences were observed after downsampling, due in large part to overlaps between the in-bandwidth (above the −10 dB level) and out-of-bandwidth (below the −10 dB level) signals. Bandpass sampling also had numerical effects resulting from lower sampling rates. For example, interpolation errors (linear interpolation was used in the beamforming algorithm) were greater with increased step sizes. Band-limited sinc interpolation would probably be a better option. Digital filtering (e.g., low-pass filtering

during I/Q demodulation) was also affected by undersampling. To sum up, bandpass sampling decreased signal-to-noise ratio through: 1) frequency overlap; 2) numerical interpolation; 3) digital filtering. Frequency overlap tends to decrease signal-to-noise ratio owing to aliasing of the out-of-band noise. Another potential source of error is frequency-dependent attenuation: the center frequency of the received signal might be different from the transmitted frequency. However, although it cannot be firmly confirmed by this paper, it is likely that those differences would have a minor impact on a physiological or clinical context whenever the bandwidth and center frequency satisfy (4). Since the signal bandwidth was as low as 15% in the disc experiments, an undersampling ratio of 13 was possible with the linear array, thus reducing the sampling frequency from 20 down to 1.5 MHz. For VFI in the carotid bifurcation, the sampling frequency was reduced down to 1.8 MHz (ratio = 11). The undersampling ratio was 5 with the adult cardiac transducer since its center frequency was lesser. We thus obtained a five- to ten-fold decrease in data storage for the Doppler applications (when excluding B-mode) investigated in this paper. As discussed earlier in the introduction, sub-Nyquist ADC sampling rates can be of particular interest in situations requiring large data volume (e.g., 3-D Doppler) or with limited transfer rates.

A. Breaking the Standard Nyquist Limit in Fast Time and Slow Time

The Nyquist-Shannon sampling theorem paper states that if a function contains no frequencies higher than $f_{\max}$, it is completely determined by uniformly spaced data sampled with a rate $2f_{\max}$ [30]. As discussed earlier, bandpass sampling or undersampling for band-limited signals is a procedure to break this Nyquist barrier. We demonstrated that RF undersampling is remarkably appropriate for ultrasound flow imaging since RF signals for color Doppler have a small bandwidth through fast time. In this paper, we also went beyond a second Nyquist limit in the slow time: we extended the Nyquist Doppler velocity, classically limited by the number of ultrasound transmissions per second (PRF). For this purpose, the pulses were transmitted through a dual-PRF scheme [22], an emission process where time delays between two successive transmissions change in an alternating way. With the arrangement applied in this paper, the Nyquist velocity was doubled; thus, no Doppler aliasing was present within the investigated velocity ranges. To make multi-PRF schemes work correctly, blood flow must be quasi-stationary during the time required to register one slow-time ensemble. This situation is not encountered in highly spatially and/or temporally fluctuating flows, such as in stenoses.

B. Other Approaches for Sub-Nyquist Sampling

In this paper, we exclusively analyzed bandpass sampling, one of the simplest approaches for sub-Nyquist sampling. Other methods have been described in the context of ultrasound imaging. Analog or digital demodulation and quadrature sampling have been the most usual techniques to reduce the sampling rate of a bandpass RF signals below the Nyquist limit [31], [32]. With the advent of digital beamforming, ultrasound RF undersampling has been recently proposed to allow the use of high-frequency transducers with a limited ADC sampling rate [10]. In undersampling, the theoretical lowest rate $2B$ of a band-limited signal (Landau's rate) can be achieved only when the upper frequency verifies $f_U = kB$, with k an integer [33]. This limit $f_s = 2B$ can be attained by using periodically nonuniform sampling [33], [34]. It seems that this approach has not been investigated by the ultrasound imaging community. More advanced techniques for sub-Nyquist sampling in ultrasound imaging have also been introduced. Assuming that RF ultrasound signals can be fully described by a relatively small number of backscattered echoes, Tur *et al.* [35] used a FRI (finite rate of innovation) framework to reduce the sampling rate below Landau's rate ($2B$). This approach has been shown to detect strong reflectors efficiently; however, it does not preserve the speckles. The same team then developed compressed beamforming in the Fourier domain to avoid the loss of speckle information [36], [37]. In the latter studies, beamforming was carried out in the frequency domain using a compressive sensing technique with a reduced number of Fourier coefficients. This compressed beamforming method is based on a constrained l_1 minimization and has been tested *in vitro* and *in vivo* with a wireless ultrasound system [38]. Whether compressed beamforming preserves phases for color Doppler and vector Doppler imaging was not investigated. Unlike analog demodulation, undersampling or periodically nonuniform sampling, data reduction in [35] and [36] occurred after ADC, in the digital front-end. This technique thus does not address the issues of high-frequency ultrasound. Furthermore, it cannot benefit from the technical advantages of undersampling ADC, which makes it a good solution for reducing power consumption and cost in handheld battery-powered scanners.

C. Application to 2-D and 3-D Doppler

Due to the relatively small bandwidth (long pulses), Doppler imaging lends itself to bandpass sampling, as was illustrated by the *in vitro* and *in vivo* results of this paper. Avoiding excessive load of data is of high interest for handheld and/or wireless point-of-care ultrasonography in remote and emergency environments. In addition, ADCs working at lower rates convert analog signals with smaller chip area and lower power dissipation, thus easing miniaturization and extending battery-operating life. Volumetric high-frame-rate echography with matrix arrays can also benefit from RF undersampling since this modality generates very large volumes of 4-D (3-D + time) data [6], [39]. Coming back to the example pointed out in the introduction and adapting it to 4-D, a 5 MHz 32×32-element matrix array and a 14-b resolution ADC, digitizing at four times the carrier frequency, would provide a RF data flow of $1024 \times 20 \times 10^6 \times 14/8 \approx 36$ GB/s. After ADC, these data must be digitally demodulated, decimated, and beamformed. RF bandpass sampling can substantially reduce the workflow toward the digital front-end, up to ~10 times for Doppler modes. In addition, it reduces data volumes for the subsequent digital signal processing tasks. RF undersampling,

or other sub-Nyquist sampling at the level of the analog front-end, could thus be a method of choice in volumetric color and vector Doppler.

D. Limitations of the Study

In this paper, the RF signals were not undersampled by the ADC. Undersampling was carried out retrospectively and artificially by downsampling the output RF signals, originally sampled at four times the center frequency. In this paper, the highest sampling rate was 20 MHz with the 5-MHz linear array. Since the A/D converters of the Verasonics V1 can only sample in the range from 20 to 60 MHz, undersampling at the ADC level would not have been possible. On the other hand, our protocol allowed direct comparisons with the gold-standard 4× sampling. The ideal protocol should include the design of circuit assemblies with undersampling ADCs. These electronic considerations, however, fall outside of our scope of expertise. Furthermore, bandpass sampling is not the optimum method for sub-Nyquist sampling since it may not reach Landau's rate ($f_s = 2B$). As discussed earlier, Landau's rate can be achieved with periodically nonuniform sampling. This paper was not designed to test this sampling method. Finally, another limitation of this paper is the idealness of the *in vitro* flow conditions. The latter were clutter free; however, it is likely that sub-Nyquist sampling has little or no impact on the clutter signals. Our *in vivo* flow findings tend to confirm this assertion.

V. Conclusion

Accurate color and vector Doppler images were obtained in plane and diverging wave imaging with RF undersampling. RF undersampling could be a method of choice to avoid data overload and reduce data workflow in 2-D and 3-D parallel ultrasound imaging.

References

[1] M. Tanter and M. Fink, "Ultrafast imaging in biomedical ultrasound," *IEEE Trans. Ultrason., Ferroelect., Freq. Control*, vol. 61, no. 1, pp. 102–119, Jan. 2014.

[2] J. A. Jensen, S. I. Nikolov, A. C. H. Yu, and D. Garcia, "Ultrasound vector flow imaging—Part II: Parallel systems," *IEEE Trans. Ultrason., Ferroelect., Freq. Control*, vol. 63, no. 11, pp. 1722–1732, Nov. 2016.

[3] E. Macé, G. Montaldo, I. Cohen, M. Baulac, M. Fink, and M. Tanter, "Functional ultrasound imaging of the brain," *Nature Methods*, vol. 8, pp. 662–664, May 2011.

[4] K. L. Hansen *et al.*, "Intraoperative cardiac ultrasound examination using vector flow imaging," *Ultrason. Imag.*, vol. 35, no. 4, pp. 318–332, 2013.

[5] J. Faurie *et al.*, "Intracardiac vortex dynamics by high-frame-rate Doppler vortography—*In vivo* comparison with vector flow mapping and 4-D flow MRI," *IEEE Trans. Ultrason., Ferroelect., Freq. Control*, vol. 64, no. 2, pp. 424–432, Feb. 2017.

[6] J. Provost *et al.*, "3D ultrafast ultrasound imaging *in vivo*," *Phys. Med. Biol.*, vol. 59, no. 19, pp. L1–L13, 2014.

[7] M. Correia, J. Provost, M. Tanter, and M. Pernot, "4D ultrafast ultrasound flow imaging: *In vivo* quantification of arterial volumetric flow rate in a single heartbeat," *Phys. Med. Biol.*, vol. 61, no. 23, pp. L48–L61, 2016.

[8] S. Holbek *et al.*, "Ultrasonic 3-D vector flow method for quantitative *in vivo* peak velocity and flow rate estimation," *IEEE Trans. Ultrason., Ferroelect., Freq. Control*, vol. 64, no. 3, pp. 544–554, Mar. 2017.

[9] A. J. Jerri, "The Shannon sampling theorem—Its various extensions and applications: A tutorial review," *Proc. IEEE*, vol. 65, no. 11, pp. 1565–1596, Nov. 1977.

[10] P. Kaczkowski, "Bandwidth sampling data acquisition with the Vantage system for high frequency transducers," Verasonics, Kirkland, WA, USA, White Paper, 2016, pp. 1–5. [Online]. Available: http://verasonics.com/wp-content/uploads/2016/07/Vantage_bandwidth_sampling_white_paper_July.2016.pdf

[11] K. Owen, M. I. Fuller, and J. A. Hossack, "Application of X-Y separable 2-D array beamforming for increased frame rate and energy efficiency in handheld devices," *IEEE Trans. Ultrason., Ferroelect., Freq. Control*, vol. 59, no. 7, pp. 1332–1343, Jul. 2012.

[12] H. Eskandari, O. Goksel, S. E. Salcudean, and R. Rohling, "Bandpass sampling of high-frequency tissue motion," *IEEE Trans. Ultrason., Ferroelect., Freq. Control*, vol. 58, no. 7, pp. 1332–1343, Jul. 2011.

[13] P. A. Hager, A. Bartolini, and L. Benini, "Ekho: A 30.3W, 10k-channel fully digital integrated 3-D beamformer for medical ultrasound imaging achieving 298M focal points per second," *IEEE Trans. Very Large Scale Integr. (VLSI) Syst.*, vol. 24, no. 5, pp. 1936–1949, May 2016.

[14] M. Mishali and Y. C. Eldar, "Sub-Nyquist sampling," *IEEE Signal Process. Mag.*, vol. 28, no. 6, pp. 98–124, Nov. 2011.

[15] C. R. Deane, F. Forsberg, N. Thomas, and V. C. Roberts, "Accuracy of colour Doppler ultrasound velocity measurements in small vessels," *J. Biomed. Eng.*, vol. 13, no. 3, pp. 249–254, May 1991.

[16] W. F. Walker and G. E. Trahey, "A fundamental limit on delay estimation using partially correlated speckle signals," *IEEE Trans. Ultrason., Ferroelect., Freq. Control*, vol. 42, no. 2, pp. 301–308, Mar. 1995.

[17] J. L. Brown, "On quadrature sampling of bandpass signals," *IEEE Trans. Aerosp. Electron. Syst.*, vol. AES-15, no. 3, pp. 366–371, May 1979.

[18] P. Tortoli, L. Bessi, and F. Guidi, "Bidirectional Doppler signal analysis based on a single RF sampling channel," *IEEE Trans. Ultrason., Ferroelectr., Freq. Control*, vol. 41, no. 1, pp. 1–3, Jan. 1994.

[19] R. G. Vaughan, N. L. Scott, and D. R. White, "The theory of bandpass sampling," *IEEE Trans. Signal Process.*, vol. 39, no. 9, pp. 1973–1984, Sep. 1991.

[20] R. G. Lyons, "Sampling bandpass signals," in *Understanding Digital Signal Processing*, 2nd ed. Englewood Cliffs, NJ, USA: Prentice-Hall, 2004.

[21] D. Garcia, L. Le Tarnec, S. Muth, E. Montagnon, J. Porée, and G. Cloutier, "Stolt's f-k migration for plane wave ultrasound imaging," *IEEE Trans. Ultrason., Ferroelect., Freq. Control*, vol. 60, no. 9, pp. 1853–1867, Sep. 2013.

[22] D. Posada *et al.*, "Staggered multiple-PRF ultrafast color Doppler," *IEEE Trans. Med. Imag.*, vol. 35, no. 6, pp. 1510–1521, Jun. 2016.

[23] T. Loupas, J. T. Powers, and R. W. Gill, "An axial velocity estimator for ultrasound blood flow imaging, based on a full evaluation of the Doppler equation by means of a two-dimensional autocorrelation approach," *IEEE Trans. Ultrason., Ferroelect., Freq. Control*, vol. 42, no. 4, pp. 672–688, Jul. 1995.

[24] M. Tanter, J. Bercoff, L. Sandrin, and M. Fink, "Ultrafast compound imaging for 2-D motion vector estimation: Application to transient elastography," *IEEE Trans. Ultrason., Ferroelect., Freq. Control*, vol. 49, no. 10, pp. 1363–1374, Oct. 2002.

[25] S. Dort, S. Muth, A. Swillens, P. Segers, G. Cloutier, and D. Garcia, "Vector flow mapping using plane wave ultrasound imaging," in *Proc. IEEE Int. Ultrason. Symp.*, Oct. 2012, pp. 330–333.

[26] B. Y. S. Yiu, S. S. M. Lai, and A. C. H. Yu, "Vector projectile imaging: Time-resolved dynamic visualization of complex flow patterns," *Ultrasound Med. Biol.*, vol. 40, no. 9, pp. 2295–2309, Sep. 2014.

[27] C. M. Hurvich and T. Chih-Ling, "Regression and time series model selection in small samples," *Biometrika*, vol. 76, no. 2, pp. 297–307, 1989.

[28] D. Garcia, "Robust smoothing of gridded data in one and higher dimensions with missing values," *Comput. Statist. Data Anal.*, vol. 54, no. 4, pp. 1167–1178, Apr. 2010.

[29] D. Garcia, "A fast all-in-one method for automated post-processing of PIV data," *Experim. Fluids*, vol. 50, no. 5, pp. 1247–1259, Oct. 2010.

[30] C. E. Shannon, "Communication in the presence of noise," *Proc. Inst. Radio Eng.*, vol. 37, no. 1, pp. 10–21, Jan. 1949.

[31] F. Forsberg and M. Ø. Jørgensen, "Sampling technique for an ultrasound Doppler system," *Med. Biol. Eng. Comput.*, vol. 27, no. 2, pp. 207–210, Mar. 1989.

[32] T. L. Szabo, *Diagnostic Ultrasound Imaging: Inside Out*. San Francisco, CA, USA: Academic, 2004.

[33] A. Kohlenberg, "Exact interpolation of band-limited functions," *J. Appl. Phys.*, vol. 24, no. 12, pp. 1432–1436, 1953.

[34] Y.-P. Lin and P. P. Vaidyanathan, "Periodically nonuniform sampling of bandpass signals," *IEEE Trans. Circuits Syst. II, Analog Digit. Signal Process.*, vol. 45, no. 3, pp. 340–351, Mar. 1998.

[35] R. Tur, Y. C. Eldar, and Z. Friedman, "Innovation rate sampling of pulse streams with application to ultrasound imaging," *IEEE Trans. Signal Process.*, vol. 59, no. 4, pp. 1827–1842, Apr. 2011.

[36] T. Chernyakova and Y. Eldar, "Fourier-domain beamforming: The path to compressed ultrasound imaging," *IEEE Trans. Ultrason., Ferroelect., Freq. Control*, vol. 61, no. 8, pp. 1252–1267, Aug. 2014.

[37] A. Burshtein, M. Birk, T. Chernyakova, A. Eilam, A. Kempinski, and Y. C. Eldar, "Sub-Nyquist sampling and Fourier domain beamforming in volumetric ultrasound imaging," *IEEE Trans. Ultrason., Ferroelect., Freq. Control*, vol. 63, no. 5, pp. 703–716, May 2016.

[38] Y. C. Eldar. (2015). *Yonina Eldar—Software & Hardware—Software Page*. [Online]. Available: http://webee.technion.ac.il/people/YoninaEldar/demo%20movies.php

[39] J. Provost, C. Papadacci, C. Demene, J. L. Gennisson, M. Tanter, and M. Pernot, "3-D ultrafast Doppler imaging applied to the noninvasive mapping of blood vessels *in vivo*," *IEEE Trans. Ultrason., Ferroelect., Freq. Control*, vol. 62, no. 8, pp. 1467–1472, Aug. 2015.